AGU PUBLICATIONS

Geochemistry, Geophysics, Geosystems

RESEARCH ARTICLE

10.1002/2016GC006421

Key Points:
- Methane seeps occur in Hudson Canyon updip of clathrate hydrate stability
- The concentration and oxidation of this methane are quantified
- The seafloor emission of methane is assessed

Supporting Information:
- Supporting Information S1
- Supporting Information S2
- Table S1
- Table S2
- Table S3
- Data Set S1
- Data Set S2
- Data Set S3

Correspondence to:
J. D. Kessler,
john.kessler@rochester.edu

Citation:
Weinstein, A., L. Navarrete, C. Ruppel, T. C. Weber, M. Leonte, M. Y. Kellermann, E. C. Arrington, D. L. Valentine, M. I. Scranton, and J. D. Kessler (2016), Determining the flux of methane into Hudson Canyon at the edge of methane clathrate hydrate stability, *Geochem. Geophys. Geosyst.*, *17*, 3882–3892, doi:10.1002/2016GC006421.

Received 28 APR 2016
Accepted 25 AUG 2016
Accepted article online 29 AUG 2016
Published online 13 OCT 2016

Determining the flux of methane into Hudson Canyon at the edge of methane clathrate hydrate stability

Alexander Weinstein[1], Luis Navarrete[1], Carolyn Ruppel[2], Thomas C. Weber[3], Mihai Leonte[1], Matthias Y. Kellermann[4], Eleanor C. Arrington[5], David L. Valentine[4,6], Mary I. Scranton[7], and John D. Kessler[1]

[1]Department of Earth and Environmental Sciences, University of Rochester, Rochester, New York, USA, [2]U.S. Geological Survey, Woods Hole, Massachusetts, USA, [3]School of Marine Science and Ocean Engineering, University of New Hampshire, Durham, New Hampshire, USA, [4]Marine Science Institute, University of California, Santa Barbara, California, USA, [5]Interdepartmental Graduate Program in Marine Science, University of California, Santa Barbara, California, USA, [6]Department of Earth Science, University of California, Santa Barbara, California, USA, [7]School of Marine and Atmospheric Sciences, Stony Brook University, Stony Brook, New York, USA

Abstract Methane seeps were investigated in Hudson Canyon, the largest shelf-break canyon on the northern U.S. Atlantic Margin. The seeps investigated are located at or updip of the nominal limit of methane clathrate hydrate stability. The acoustic identification of bubble streams was used to guide water column sampling in a 32 km^2 region within the canyon's thalweg. By incorporating measurements of dissolved methane concentration with methane oxidation rates and current velocity into a steady state box model, the total emission of methane to the water column in this region was estimated to be 12 kmol methane per day (range: 6–24 kmol methane per day). These analyses suggest that the emitted methane is largely retained inside the canyon walls below 300 m water depth, and that it is aerobically oxidized to near completion within the larger extent of Hudson Canyon. Based on estimated methane emissions and measured oxidation rates, the oxidation of this methane to dissolved CO_2 is expected to have minimal influences on seawater pH.

1. Introduction

Ocean clathrate hydrates contain an enormous global reservoir of the greenhouse gas methane (CH_4) [*Milkov*, 2004] and the partial destabilization of this reservoir has been suspected to have influenced past climate through the release of globally significant quantities of CH_4 carbon [e.g., *Dickens et al.*, 1995; *Kennett et al.*, 2000]. Since the stability of these structures is controlled by pressure, temperature, and the availability of CH_4 [*Dickens and Quinby-Hunt*, 1994], hypotheses have been advanced suggesting a positive climatological feedback between changing ocean temperature and CH_4 release from oceanic clathrate hydrates [*Archer*, 2007; *Ruppel*, 2011]. However, measuring this feedback is a challenge. Most investigations of clathrate hydrates have been conducted along active continental margins where the stability of hydrates is controlled in part by connections with the deeper geosphere [*Jerram et al.*, 2015; *Milkov et al.*, 2004; *Tréhu et al.*, 2004]. Passive continental margins largely remove connections to the deeper geosphere, enabling more constrained investigations between clathrate stability and changing ocean temperature. The recent discovery of extensive seepage at upper continental slope depths shallower than (updip from) the shallowest limit of methane hydrate stability along the northern U.S. Atlantic margin (USAM) provides a relatively accessible, midlatitude passive margin on which to test CH_4 clathrate hydrate-climate connections [*Kessler*, 2014; *Skarke et al.*, 2014; *Brothers et al.*, 2014]. While CH_4 seepage and clathrate stability have been investigated along passive continental margins in the Arctic [e.g., *Graves et al.*, 2015; *Mau et al.*, 2013; *Westbrook et al.*, 2009], the USAM is the first discovery of such expansive seepage at or near the boundary of clathrate stability outside of these high-latitude regions.

Here we determine fluxes of CH_4 into the water column at the upper edge of CH_4 hydrate stability along the main axis (i.e., thalweg) of Hudson Canyon. This study area was chosen not only because the CH_4 seep sites lie close to the theoretical updip limit of gas hydrate stability on the USAM [*Skarke et al.*, 2014], but also because the CH_4 dissolved in seawater can accumulate to higher concentrations due to the restricted circulation caused by the canyon walls [*Pierdomenico et al.*, 2015; *Rona et al.*, 2015]. Fluxes of CH_4 from the

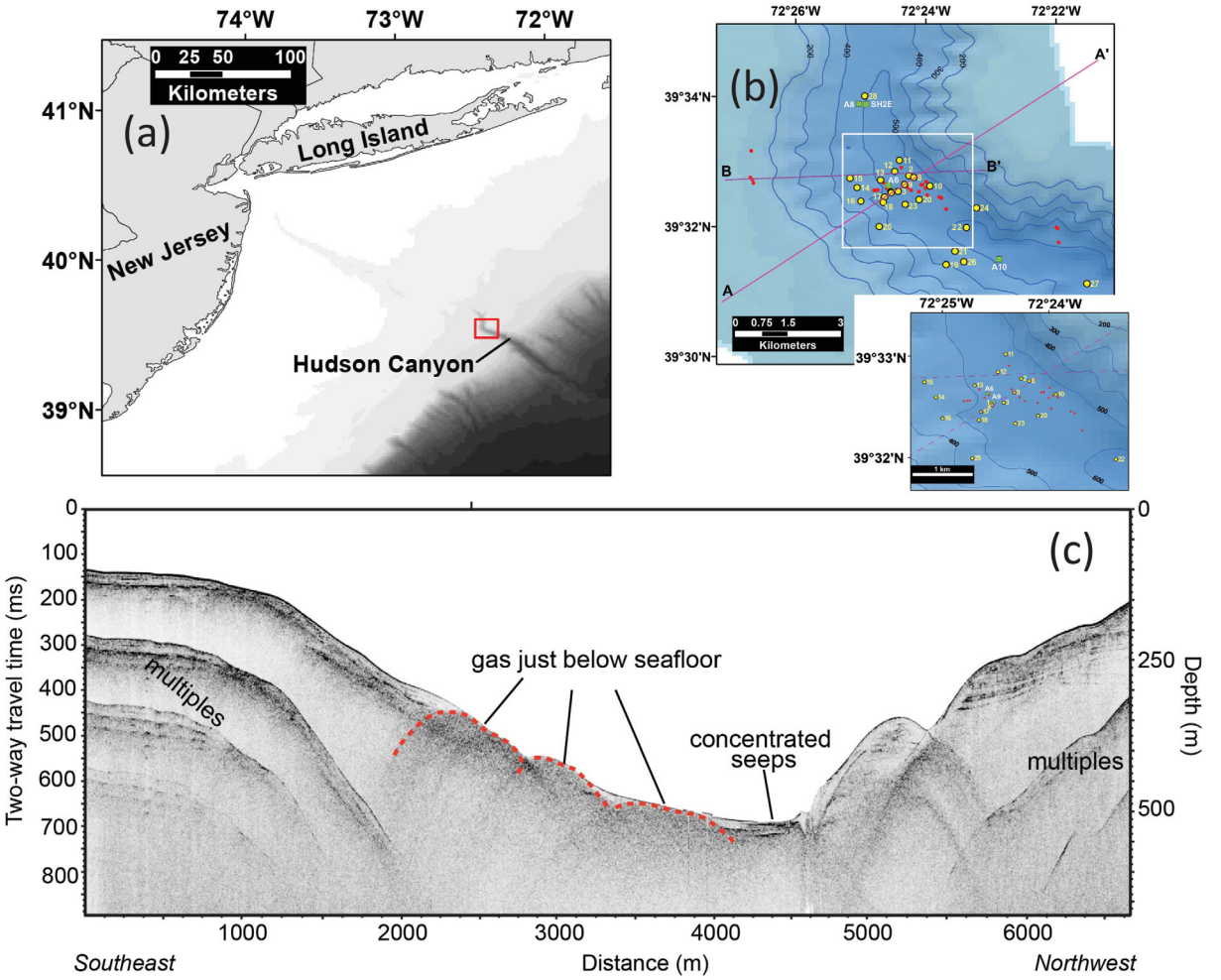

Figure 1. (a) Samples were collected in Hudson Canyon, northern U.S. Atlantic margin (USAM) from the 9 to 13 July 2014. (b) Water column sampling sites (CTD hex file numbers) in Hudson Canyon, superposed on a bathymetric map from [*Butman et al.*, 2006]. The red circles are previously identified CH_4 seeps [*Skarke et al.*, 2014]. Line A-A′ is the canyon cross section used to formulate 3-D boxes for the steady state model. Line B-B′ is the transect for the subbottom profile data. (c) Subbottom profile collected with a towed Edgetech 512i Chirp acoustic system in September 2015 shows the presence of gas and the seafloor structure beneath the area of concentrated gas seeps.

seafloor were determined using a vertical box modeling approach, adapted from previous work [*Kessler et al.*, 2005, 2006a, 2006b; *Scranton*, 1988; *Scranton et al.*, 1987]. Supported by numerous CH_4 concentration profiles measured over a 5 year period, the modeling approach assumes steady state and uses measured vertical profiles of dissolved CH_4 concentration, CH_4 oxidation rates, and current velocity to determine seafloor emissions.

2. Materials and Methods

2.1. Data and Sample Collection

Data and samples were collected in the thalweg of Hudson Canyon from 9 to 13 July 2014 on the R/V *Endeavor* (Figure 1). Based on previous discovery of CH_4 seepage in the thalweg of Hudson Canyon between 500 and 550 m water depth [*Skarke et al.*, 2014], an area approximately 6.5 km by 4.9 km centered on 39° 32.03′N, 72° 24.03′W was selected as the focus for this study. At the time of this investigation, the 500–550 m depth range that was the focus of most of the surveys and sampling lay close to the theoretical updip limit of stability for pure CH_4 hydrate in equilibrium with nominal seawater based on calculated hydrostatic pressures and measured bottom water temperatures.

Bubble plumes emanating from the sediment into the water column were detected acoustically and used to guide sampling. Acoustic anomalies in the study area were mapped using echo sounding methods

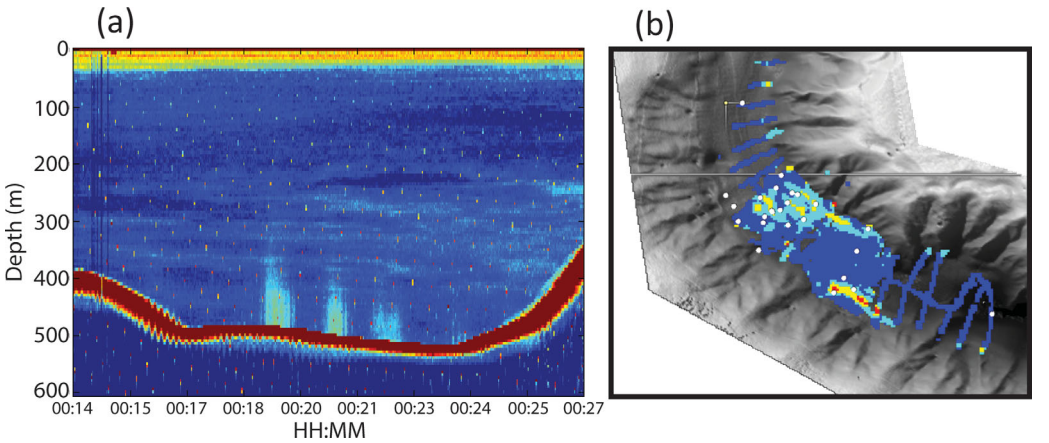

Figure 2. (a) An echogram from a cross-canyon transect, with cooler colors showing regions of low backscatter and warmer colors showing regions of high backscatter. Three distinct regions showing acoustic anomalies consistent with CH_4 gas bubbles rising from the seabed can be seen between 00:18 and 00:23. The stippling in the image is caused by interference from a subbottom profiler. The horizontal banding is consistent with acoustic scattering from marine organisms. (b) Observed acoustic anomalies within the study area: dark blue corresponds to the background (no bubble plumes observed); light blue corresponds to the smallest detectable amount of bubbles; yellow is twice the smallest amount; red is four times the smallest amount. CTD locations are shown as white circles, and bathymetry is shown in gray scale [*NOAA National Centers for Environmental Information*, 2004].

similar to those used by previous investigators [e.g., *Greinert et al*., 2006; *Hornafius et al*., 1999; *Merewether et al*., 1985; *Skarke et al*., 2014; *Weber et al*., 2014]. For this study, a 38 kHz transducer (Simrad ES38-10) was installed in the hull of the R/V *Endeavor*. The ES38-10 was used with a Simrad wideband transceiver (WBT) and transmitted linear frequency modulated acoustic signals with a nominal frequency range of 25–50 kHz. The 3 dB beam width (beam opening angle) of the ES38-10 is nominally 10°, corresponding to a 90 m sampling resolution (in the horizontal) at 500 m water depth and 70 m at 400 m water depth. The ES38-10 was used during four survey periods that were interspersed with the water sampling activities. All of the survey lines were run in the cross-canyon direction, including three at a line spacing of 50 m and one survey at a line spacing of 500 m. The recorded acoustic return from the ES38-10 was match-filtered [*Burdic*, 1991] using an ideal replica of the transmit signal and used to create echograms similar to that shown in Figure 2a. Acoustic anomalies consistent with CH_4 gas bubbles were found throughout the region, rising approximately 100 m above the seabed (Figure 2a). To create a map of gas seepage, the acoustic backscatter in each acoustic "ping" was averaged between 450 m water depth and 20 m above the seafloor. The average acoustic backscatter was gridded at 100 m × 100 m resolution and used to coarsely identify four different regions of seep intensity containing (1) the background level (no seep anomaly observed), (2) three decibels above the background level (corresponding to the weakest observed seep anomaly), (3) six decibels above the background level, and (4) nine decibels above the background level (Figure 2b). In the areas assumed to contain methane bubbles, the acoustic backscatter intensity is assumed to be proportional to the number of bubbles present in the water column with the underlying assumption that the bubble-size distributions are similar. The four classified regions are therefore assumed to correspond to no bubbles, the smallest detectable amount of bubbles, twice the smallest amount, and four times the smallest amount, and corresponded to surveyed areas of 23.7, 6.6, 1.8, and 0.4 km^2, respectively (Figure 2b). These areas, along with the corresponding locations where water samples were collected, were used to create spatially weighted averages of the measured results, as detailed below.

The presence and absence of acoustically detected bubble plumes was used to direct water sampling using a rosette of 24 Niskin bottles. Samples for CH_4 concentration analyses were collected by filling 60, 120, or 160 mL glass serum vials. Vials were filled from the bottom with a length of $^1/_4$″ Tygon tubing. Vials were flushed with seven vial volumes of seawater to expel any bubbles and ensure collection of a clean sample, and then were sealed with butyl rubber stoppers taking care not to introduce bubbles during sealing. Immediately after sealing, a 10 mL headspace of ultrahigh purity nitrogen was introduced, displacing an equal volume of water, and the samples were preserved by adding 25 μL of a saturated solution of mercuric chloride. The vials were stored inverted to minimize diffusive gas exchange through the butyl rubber stopper. All the concentration analyses were conducted at the University of Rochester using a gas

chromatograph with a flame-ionization detector (GC-FID; Agilent 6850). At least 24 h prior to analysis, the vials were stored inverted in a 6°C incubator to mimic in situ conditions and help maintain atmospheric pressure inside the vials. Five mL of the headspace gas were removed from each vial via displacement with an equal volume of CH_4-free water and used to flush and fill a 50 μL sample loop on the GC-FID. The contents of the sample loop were transferred into the GC-FID to determine the CH_4 concentration. The headspace concentration was converted into the original dissolved CH_4 concentration using the known solubility of CH_4 [*Wiesenburg and Guinasso*, 1979], the temperature of the incubator, the salinity of the water as determined by CTD, and the volumes of the headspace and water in each vial. The GC-FID was calibrated with five gaseous standards bracketing the sample headspace concentration. Blanks and standards were analyzed interspersed with the samples, indicating that (1) the storage of samples prior to analysis did not alter the concentrations when following these protocols; and (2) blanks showed no detectable concentrations of CH_4. The average precision determined from replicate natural samples collected in different vials by different analysts was 5.2%; this precision was not influenced by sample concentration and is similar to what was determined elsewhere [*Valentine et al*., 2010; *Yvon-Lewis et al*., 2011]. The detection limit of this technique as determined by combining the instrumentation detection limit and the water sampling and preparation procedures outlined above was 0.5 nM.

Methane oxidation rate measurements were conducted using a stable isotope tracer technique. Seawater samples were collected in 160 mL glass serum vials, following similar protocols to the CH_4 concentration analyses. After collection, the samples were placed in an 8°C incubator to become isothermal, 50 μL of pure $^{13}CH_4$ was added to each vial with a high-precision Hamilton syringe without adding additional gaseous headspace, and the vials were incubated for a predetermined amount of time, which ranged from 1 to 2 days, to assess the influence of incubation time on oxidation rate determined. The incubation was terminated with the addition of a saturated solution of mercuric chloride. All incubations were conducted in triplicate with blanks (no added $^{13}CH_4$ tracer) and "killed" ($^{13}CH_4$ and mercuric chloride added at the start of the incubation) controls. The oxidation rate was determined from the original amount of the stable isotope tracer added and the amount transferred to a dissolved inorganic carbon (DIC) product (assuming a 1:1 stoichiometry) over the duration of the incubation. This procedure for determining oxidation rates ignores incorporation of $^{13}CH_4$ into biomass, and this potential source of uncertainty is assessed with a sensitivity analysis in the modeling studies below. Methane oxidation was treated as following both pseudo-first-order and zeroth-order kinetics in our flux modeling studies.

Current velocity was measured with an acoustic Doppler current profiler (ADCP), RDI 75 kHz Ocean Surveyor, mounted on the hull of the R/V *Endeavor*. This ADCP was operated in narrowband mode using two different configurations based on scientific needs. When data acquisition from a different sonar system, ES38-10, was most important, the ADCP was externally triggered and configured to use 8 m bins with 8 m blanking distance. Under normal operating conditions when the ES38-10 was not used, the ADCP was triggered internally and used 16 m bins with 8 m blanking. ADCP data were processed using the University of Hawaii's Data Acquisition System (UHDAS). The shallowest depth measured by the ADCP was roughly 30 m and measurements were determined every 8 or 16 m to the seafloor, based on the bin distance used. The average uncertainty of the recorded ADCP data was 0.02 m s^{-1}.

2.2. Flux Modeling

The modeling approach employed here is based on previous time-dependent and steady state models of seawater CH_4 concentration [*Kessler et al*., 2005, 2006a, 2006b; *Scranton et al*., 1987; *Scranton*, 1988]. Here, the model assumes the concentration of dissolved CH_4 in the water column is in steady state and thus the source of CH_4 to this region can be determined based on the amount necessary to balance the sum of CH_4 losses. The steady state assumption was tested by comparing the water column concentration of CH_4 determined here in July 2014 against similar profiles collected in 2009 and 2011 [*Rona et al*., 2015]. No significant changes were observed in the magnitude or morphology of these vertical water column CH_4 distributions (Figure 3a). While shorter-term concentration variations may occur, the available data suggest that the dissolved CH_4 concentration in Hudson Canyon water column is roughly in steady state on annual timescales.

The study region in the thalweg of Hudson Canyon is represented in this model as a vertical stack of six, three-dimensional boxes (Figure 4). The six boxes describing this model were restricted to depths showing CH_4 concentrations above background (i.e., $>$275 m). While lateral changes in CH_4 concentration were observed in this region related to proximity to active seepage (Figures 1–3), this approach models only vertical changes in concentration and assumes that each depth range can be represented by an average of measured

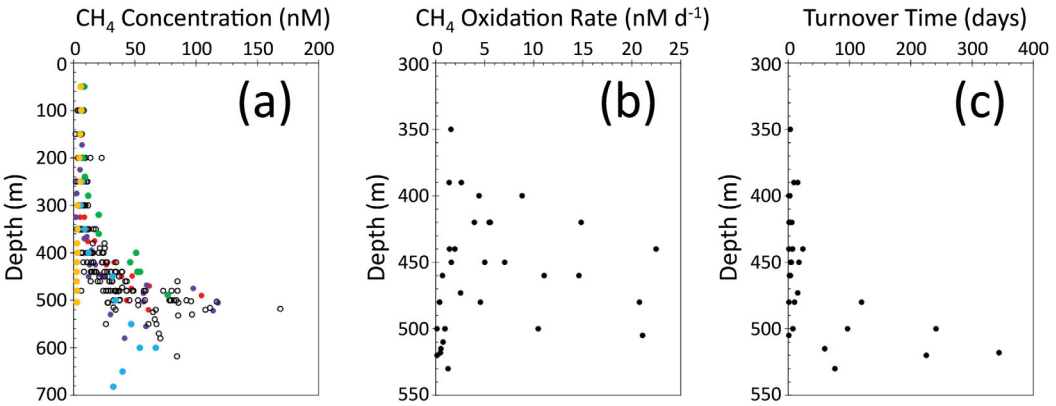

Figure 3. (a) Dissolved CH_4 concentration profiles (nM). All profiles were collected from 9 to 13 July 2014 unless otherwise indicated. The uncertainty of the June 2014 data is ±5.2% but is excluded from the figure for visual clarity. All profiles were collected inside Hudson Canyon except the orange circles. Black circles = Stations 1, 8–13, 15–16, and 18–26. Orange circles = Station 6, collected outside Hudson Canyon at a comparable depth on the upper continental slope. Green circles = Station 28, collected shoreward of the investigated seep field. Blue circles = Station 27, collected seaward of the investigated seep field. Red circles = Stations A6 and SH2E, collected in 2009 [*Rona et al.*, 2015]. Purple circles = Stations A8, A9, and A10, collected in 2011 [*Rona et al.*, 2015]. Two additional samples are not displayed due to their relatively high concentration: (2011, Station A10, Depth = 505 m, CH_4 concentration = 224 nM) (2014, Station 8, Depth = 522 m, CH_4 concentration = 335 nM). (b) CH_4 oxidation rates (nM d^{-1}) collected inside Hudson Canyon seep field. (c) The CH_4 turnover time due to CH_4 oxidation. Since the CH_4 oxidation rates are not correlated with depth, the longer turnover times in the deep waters are due to the higher concentrations of CH_4.

values. The volume and cross-sectional areas of each box were estimated as follows. First, bathymetric data were obtained from the US Coastal Relief Model Grids available at the National Geophysical Data Center (https://www.ngdc.noaa.gov/). Since the goal was to mimic the gross morphology of this region, using finer-resolution bathymetric grids is not expected to alter the calculations or results obtained here. A region encompassing this seep site (39.48–39.59°N, 72.32–72.47°W) was exported to a database and reprojected to the Universal Transverse Mercator (UTM) coordinate system to analyze distance relationships. Second, a vertical cross-section perpendicular to the thalweg was chosen by the line intersecting the majority of stations where water samples were collected (Figure 1b). Third, the shape of this cross-section was simplified into a basic triangle and combined with the lengths of our study area running parallel to the canyon to create a triangular prism. The prism was subdivided into six 50 m high boxes inside the canyon walls (Figure 4a). Uncertainties associated with using a triangular prism to represent the volume inside Hudson Canyon are insignificant compared to other uncertainties detailed below. Using this representation allowed for the area of canyon walls (Aw_i; m^2), cross-sectional areas of the canyon perpendicular to the thalweg (Ac_i; m^2), and volume of each vertical box (V_i; m^3) to be accounted for in the CH_4 flux model (Figure 4b), where the subscript i refers to the specific box number. The measurements of CH_4 concentration (C_i; mol m^{-3}), CH_4 oxidation rate (MOx_i; moles m^{-3} d^{-1}), and current speed (Cs_i; m d^{-1}) were averaged over the depth interval z_i (m) of each individual box (box_i); both unweighted and weighted averages were calculated and used in the model. The weighted averages of C_i, MOx_i, and Cs_i were calculated using the seafloor areas of the four different seep intensity regions to account for the spatial as well as intensity heterogeneity of seafloor seeps (Figure 2b).

This model constrains CH_4 losses from each box via vertical diffusion (*Dif*), horizontal advection (*Adv*), and biological oxidation (*Ox*), each with units of mol d^{-1} (Figure 4b and equation (1)). The input of CH_4 (mol d^{-1}) into each box can be determined as the sum of the loss terms (*Dif*, *Adv*, and *Ox*) for each box, and the flux (mol m^{-2} d^{-1}) or volume input rate (nmol L^{-1} d^{-1}) can be determined by dividing the input by Aw_i or V_i, respectively. However, we view the input rates (mol d^{-1} or nmol L^{-1} d^{-1}) to be more accurate than flux (mol m^{-2} d^{-1}), since a bubble of CH_4 may be emitted to the water column outside of box_i (i.e., not associated with Aw_i) and propagate vertically until it fully dissolves in a specific box. This modeling approach is similar to what was used previously [*Kessler et al.*, 2006a, 2006b; *Scranton*, 1988]; however, the influence of advection on CH_4 concentrations was also considered here:

$$\frac{dCH_4}{dt} = Sources - Dif - Adv - Ox = 0 \quad (1)$$

Vertical diffusion was modeled following Fick's first law of diffusion:

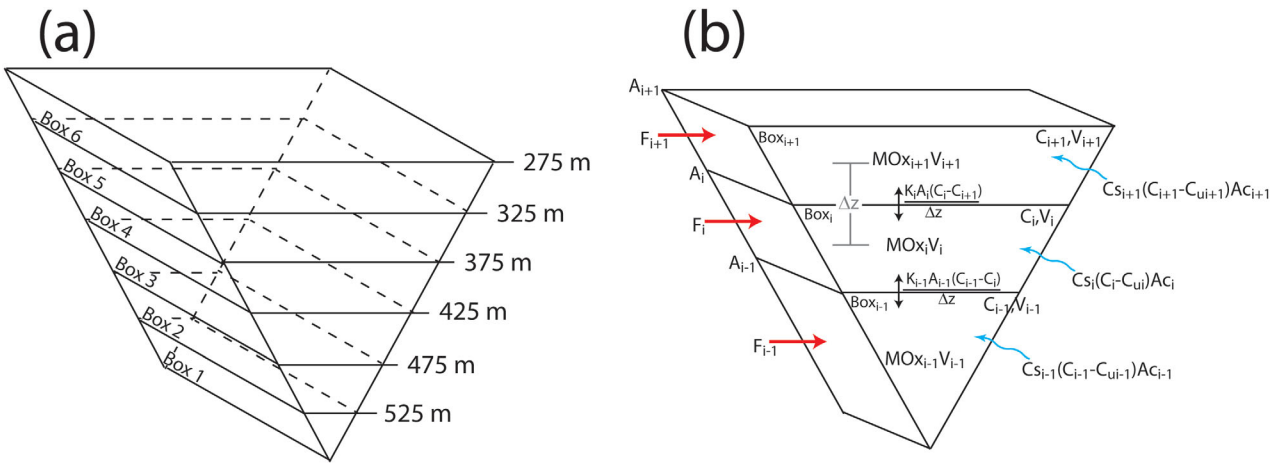

Figure 4. (a) Illustration of the box model. Depth labels show meters below sea level. Left and right faces characterize contact with canyon walls. The open ocean occurs at depths <175 m, thus all boxes are contained within the canyon. (b) Schematic of the sources and sinks of CH_4 for each box.

$$Dif = \frac{K_i A_i (C_i - C_{i+1})}{\Delta z} \tag{2}$$

and is constrained across both the top and bottom of each box (Figure 4b). Here, K_i is the diffusion coefficient ($m^2\ d^{-1}$), Δz (m) is the height of box_i, and A_i (m^2) is the cross-sectional area of the top of box_i. Values for K_i were chosen based on values used previously [*Kessler et al.*, 2006a, 2006b; *Scranton*, 1988]; however, a sensitivity study described below illustrates that calculated input fluxes are insensitive to the values of K_i.

Horizontal advective additions and losses of CH_4 are calculated using:

$$Ad_i = Cs_i (C_i - C_u) Ac_i \tag{3}$$

where Cs_i (m d^{-1}) is the speed of water currents moving through the region and C_u is the concentration of dissolved CH_4 upstream, which is flowing into the study area. The current speed and direction were determined from the ADCP data, and current direction was used to define the region which was upstream.

Methane oxidation was modeled as following either zeroth or first-order kinetics.

$$\text{Zeroth-order kinetics}: \quad Ox_i = MOx_i V_i \tag{4}$$

$$\text{First-order kinetics}: \quad Ox_i = k_i C_i V_i \tag{5}$$

MOx_i is the zeroth-order oxidation rate in box_i in units of mol $m^{-3}\ d^{-1}$ and k_i is the first-order oxidation rate constant in box_i in units of d^{-1}. Average values of MOx_i for each box were determined by weighting the oxidation rate to the relative areas of seeps with different emission intensities (Figure 2b). To determine k_i for each box, these weighted averages of MOx_i were divided by weighted averages of C_i. Measurements of CH_4 oxidation rates were conducted in boxes 2–4 (Figure 4a). Oxidation rates (when assuming zeroth-order kinetics) or rate constants (when assuming first-order kinetics) in boxes 1 and 5 were assumed to be the same as in boxes 2 and 4, respectively.

3. Data and Results

3.1. Measurements

Above 300 m water depth, the measured concentrations were similar to the background station. However, deeper than 300 m, the concentration values increased, reaching a weighted average concentration of 68 nM in the waters of the deepest box (Figure 3a). The maximum value measured was 335 nM, most likely representing a water sample collected closest to a site of CH_4 emission. Samples collected in 2009 displayed similar trends in both vertical profile shape and magnitude [*Rona et al.*, 2015] suggesting that, at least on time scales of years, the dissolved CH_4 concentration in the water column remains relatively steady state (Figure 3a).

Water column profiles of dissolved CH_4 concentration were also measured in Hudson Canyon both landward and seaward of the main seep field (Figure 1b) in order to constrain the change in concentration with distance from the observed seep field. However, these profiles displayed dissolved CH_4 concentrations similar to those measured in the main seep field (Figure 3a), even though they were 2–3 km from the dominant sources of CH_4 (Figures 1b, 1c, and 2b). While we are unaware of extensive seepage outside of the areas investigated, currents could help to distribute the observed CH_4 injections. Previous measurements of current speed and direction determined that the deep water currents in Hudson Canyon regularly change direction due to tidal influences [*Rona et al*., 2015]. These oscillating currents most likely distribute the elevated CH_4 concentrations to these landward and seaward stations. The current speed and direction measurements that we acquired via ADCP also displayed this oscillating nature; however, when averaged over the 4 day period over which the samples were collected, a gradual, longer-term current down canyon (heading south east) was detected (supporting information Figure S1). Nonetheless, a decrease in dissolved CH_4 concentration with distance from the seep field was not observed in the data collected in 2014, suggesting that over the area observed, the CH_4 oxidation rates are slow relative to the overprinting from serial exposure to seepage during tidal oscillations [*Valentine et al*., 2012]. One additional dissolved CH_4 concentration profile was collected outside of Hudson Canyon on the upper continental slope; unlike the other stations, this water column profile displayed no noticeable CH_4 concentration increase in the deeper waters (Figure 3a) and served as a background CH_4 concentration profile in an area free of CH_4 seep influence [*Skarke et al*., 2014].

The CH_4 oxidation rate measurements were conducted in water depths that were noticeably impacted by seep emissions, as determined by elevated concentrations of dissolved CH_4 (i.e., depths greater than 325 m). Most measurements of CH_4 oxidation using an isotopic tracer assume that the rates follow first-order reaction kinetics, especially when relatively low amounts of the isotopic tracer are added [*Pack et al*., 2011]. However, it was necessary to add a relatively large amount of the $^{13}CH_4$ tracer to our samples in order to detect a noticeable isotopic change in the DIC product. For example, the dissolved CH_4 concentration before inoculating these samples with $^{13}CH_4$ ranged from 5.7 to 168.6 nM. After the $^{13}CH_4$ tracer was added, the dissolved concentration increased to 12.8 μM. Due to the large increase in CH_4 concentration, we treated these rates as following both first and zeroth-order kinetics in the seafloor flux model.

The CH_4 oxidation rates produced from this experiment were surprisingly fast, ranging from 0.14 to 22.5 nM d^{-1} (average = 5.6; standard deviation = 6.6 nM d^{-1}) (Figure 3b). While rates of this magnitude have been observed in other global oceanic environments, they are in the upper range of previously measured values [*Mau et al*., 2013 and references therein]. The turnover time (ambient CH_4 concentration divided by oxidation rate) was also fast, with average values of 7.4 days (range 1.3–24.0 days) for depths less than or equal to 450 m and 86 days (range 1.3–344.0 days) for depths greater than 450 m (Figure 3c). Since the CH_4 oxidation rates do not show a trend with depth (Figure 3b), this increase in turnover time is controlled by the higher concentrations in the deeper waters. We were initially skeptical of the fast rates of CH_4 oxidation determined here due to the relatively large amount of tracer added. However, a complementary study was conducted to determine CH_4 oxidation rates in this area without the addition of an isotopic tracer [*Leonte et al*., 2014]. This study only investigated the naturally occurring CH_4 and determined oxidation rates based on the stable isotopic fractionation of natural CH_4. Beyond suggesting that the source of methane released from this seep field is biological, the oxidation rates determined from this complementary study are in agreement with those produced here [*Leonte et al*., 2014]. One possible explanation for these rapid rates is an autoinoculation effect from repeat exposure to seep CH_4 inputs resulting from the tidal oscillations [*Valentine et al*., 2012].

3.2. Model

The steady state box model quantified the input of CH_4 into boxes 1–5, corresponding to a depth range of 325–575 m. Methane inputs to boxes above the deepest box are best viewed as a result of emission of bubbles from greater depth that did not dissolve fully until reaching this higher elevation. Since mixing due to tidal oscillations caused the dissolved CH_4 concentration in the landward and seaward stations (stations 27 and 28) to be indistinguishable from the concentrations measured in the main seep field (Figure 3a), the along canyon advection term (equation (3)) became zero and thus did not influence the emission estimates (equation (1)). In addition, due to the negligible horizontal gradients in CH_4 concentration, horizontal turbulent diffusion could not be calculated. Since CH_4 loss outside of the region investigated here cannot be

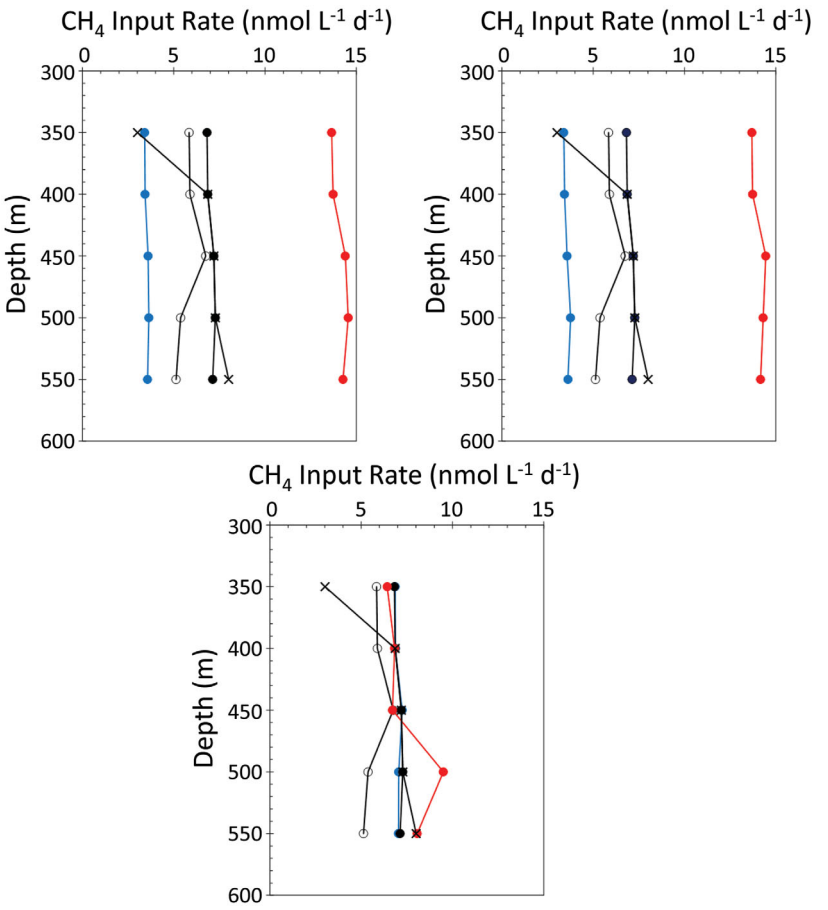

Figure 5. Model results for estimated CH_4 inputs (nmol L^{-1} d^{-1}) into Hudson Canyon as a function of depth. (a) Range of CH_4 inputs determined by increasing (red) and decreasing (blue) the aerobic CH_4 oxidation rates and diffusion coefficients by factors of 2. The solid circles incorporated the weighted averages of CH_4 concentration and oxidation rate data, while the open circles incorporated unweighted averages. All symbols incorporated CH_4 oxidation rates following zeroth-order kinetics, except the black cross which are the weighted averages following first-order kinetics. (b) and (c) Sensitivity of modeled CH_4 inputs to microbial oxidation rates (b) and diffusion coefficients (c). In Figure 5b, each model parameter was increased (red) and decreased (blue) by a factor of 2 while keeping the diffusion coefficient constant. In Figure 5c, the diffusion coefficient was increased (red) and decreased (blue) by a factor of 10.

determined, the emissions estimated here are likely underestimates and specific for the area investigated. However, these estimates were extrapolated to the full extent of the canyon in an attempt to provide some constraint on the full emission rate of CH_4.

The sensitivity of the model was tested by both increasing and decreasing the CH_4 oxidation rate (MOx_i) and eddy diffusion constant (K_i) for each box by a factor of 2 and recalculating the seep CH_4 emissions. This exercise also helps to account for natural variations, for example in MOx_i, which may be influenced by changes in the conversion efficiency of CH_4 to biomass and DIC. As would be expected from equation (1), the effect of increasing or decreasing all of the model parameters simultaneously by factors of 2 caused the

Table 1. Estimated Inputs of CH_4 to Hudson Canyon at the Edge of the CH_4 Clathrate Hydrate Stability Zone[a]

Box	Depth of Middle of Box	Low Estimate (kmol d^{-1})	Base Estimate (kmol d^{-1})	High Estimate (kmol d^{-1})
1	550	0.2	0.5	0.9
2	500	0.7	1.5	2.9
3	450	1.2	2.4	4.9
4	400	1.6	3.3	6.6
5	350	2.1	4.2	8.4
	Total	5.8	11.9	23.7

[a]The low and high inputs were estimated by decreasing and increasing K_i and MOx_i by factors of 2. All values presented incorporated weighted averages of CH_4 concentration and oxidation rates following zeroth-order kinetics.

Table 2. Sensitivity of the Cumulative CH_4 Inputs in Hudson Canyon to Modeled Parameters[a]

Test	kmol d^{-1}	Mg y^{-1}	nM d^{-1}
Normal K_i, MOx_i, Cs_i	11.8	69.2	7.0
$K_i \times 2$	11.9	69.2	7.0
$K_i/2$	11.8	69.2	7.0
$K_i \times 10$	11.9	69.6	7.0
$K_i/10$	11.8	69.1	7.0
$MOx_i \times 2$	23.7	138.3	13.9
$MOx_i/2$	5.9	34.6	3.5
K_i, $MOx_i \times 2$	23.7	138.4	13.9
K_i, $MOx_i/2$	5.9	34.6	3.5

[a]All values presented incorporated weighted averages of CH_4 concentration and oxidation rates following zeroth-order kinetics.

predicted seep CH_4 inputs to also increase or decrease by a factor of 2 (Figure 5a and Table 1). The effect of each model parameter on the predicted seep CH_4 inputs was also assessed by individually varying that particular parameter by a factor of 2 while holding all other parameters constant. An additional experiment was conducted where K_i was both increased and decreased by a factor of 10 while holding MOx_i constant (Figures 5b, 5c and Table 2). These sensitivity tests demonstrated that the seep CH_4 inputs were insensitive to changes in diffusion, but were significantly influenced by variations in CH_4 oxidation, a finding that is in line with microbial oxidation being the largest removal mechanism of CH_4 (Table 2 and Figure 5). Using weighted or unweighted averages of CH_4 concentration and oxidation rate to calculate seep emissions did produce different results; however, their differences were relatively minor compared to changes in CH_4 oxidation rates (Figure 5). In addition, the use of zeroth or first-order kinetics to describe CH_4 oxidation rates had minimal influence on the total CH_4 emission from this seep field. However, incorporating first-order kinetics did decrease the CH_4 input into box 5 due to the lower CH_4 concentration in box 5 relative to box 4 (Figure 5). In sum, the model suggests that seep CH_4 inputs below 325 m in this Hudson Canyon seep field likely average 3.5–13.9 nM d^{-1} and that the total emission of seep CH_4 in this 32 km^2 area likely ranges from 35 to 138 Mg CH_4 y^{-1}.

4. Discussion

This investigation combined measurements of dissolved CH_4 concentrations, CH_4 oxidation rates, and current velocities into a steady state model to predict CH_4 emission into the water column in Hudson Canyon at the edge of CH_4 clathrate hydrate stability. This estimate of CH_4 inputs is based on balancing measured CH_4 sinks, and thus these emission estimates can be sensitive to temporal changes in these sinks, as well as to any measurement artifacts. For this reason, we have varied the CH_4 oxidation rates and diffusion coefficients in order to provide conservative bounds on the seep CH_4 emissions. This analysis suggests that on average 69 (35–138) Mg CH_4 y^{-1} is being emitted at the updip limit of clathrate hydrate stability in Hudson Canyon. Tidal currents cause this emitted CH_4 to be dispersed both up and down the canyon beyond the area we investigated. Since this analysis determines CH_4 inputs as those necessary to balance the CH_4 sinks (equation (1)), and since CH_4 oxidation is the dominant sink (Table 2 and Figure 5), additional CH_4 oxidation that may take place outside of the area investigated will cause this emission estimate to increase. For this reason, we view these emission estimates to be lower limits on the true emission. When divided by the area experiencing CH_4 release in this study area (8.8 km^2; Figure 2b), a seafloor methane flux of 8 g CH_4 m^{-2} y^{-1} (4–16 g CH_4 m^{-2} y^{-1}) is determined. This flux is similar to mean seafloor fluxes determined previously from other marine seeps or approximately 2% of the flux from Coal Oil Point [*Hornafius et al*., 1999; *Hovland et al*., 1993].

A previous study measured dissolved CH_4 concentration further up and down canyon from this seep field [*Rona et al*., 2015]. However, many of these previous stations were along the walls of the canyon making it challenging to determine the true extent of water impacted with CH_4 from this seep field. Nonetheless, these previous data do suggest that a distance along the thalweg roughly two times greater than was investigated here could be impacted by seep CH_4. This would further increase the input to a total of 70–280 Mg CH_4 y^{-1}. These values for Hudson Canyon alone are approximately equal to the upper estimates of *Skarke et al*. [2014] for methane emissions (15–90 Mg y^{-1}) for all the newly discovered seeps between Cape Hatteras and Georges Bank. The disparity may be largely accounted for by the differences between the bottom-up approach taken by *Skarke et al*. [2014], who relied on observations of bubble emission characteristics at a few seeps to infer methane emissions at hundreds of seeps. In contrast, we use a top-down approach that relies on measured CH_4 concentrations in the water column, CH_4 oxidation rates, and a model that incorporates chemical and physical parameters to infer much larger emissions from CH_4 seeps. In addition, our

investigation identified other CH_4 seeps (Figure 2b) not previously identified in *Skarke et al*. [2014] and also accounted for dissolved CH_4 emissions from the seafloor. All of these reasons possibly contribute to the differences in emission estimates and suggest that CH_4 emission may be even more intense along the northern USAM than originally thought.

Based on the results of this study, we hypothesize that the emission and oxidation of CH_4 at the upper feather-edge of hydrate stability along the USAM [*Skarke et al*. 2014] could noticeably impact ocean chemistry. *Skarke et al*. [2014] acoustically identified over 550 CH_4 seeps along the USAM, the majority of which occurred in a region stretching 400 km between Wilmington Canyon and Cape Hatteras and located updip of the upper limit of CH_4 clathrate stability. If the seafloor CH_4 emissions and extent of CH_4 oxidation between Wilmington Canyon and Cape Hatteras are similar to what we report for Hudson Canyon, the aerobic oxidation of CH_4 from this extensive region of CH_4 emission could have significant influences on the dissolved inorganic carbon chemistry. Since the terminal product of aerobic CH_4 oxidation is CO_2 and the general direction of current flow in this region is toward the south [*Lentz*, 2008a, 2008b; *Warner et al*., 2010], if the inputs of CH_4-derived CO_2 accumulate in a parcel of water advecting between Wilmington Canyon and Cape Hatteras, the dissolved CO_2 concentration could potentially double depending on the degree of dilution. Such phenomenon could have substantial influences on the pH and buffer capacity of seawater, and potentially lead to the release of CH_4-derived CO_2 to the atmosphere. This hypothesis is based on crude extrapolations assuming that Hudson Canyon represents average CH_4 input rates and oxidation efficiencies along the USAM, and that dilution is minimal. The adequate testing of this hypothesis will require further estimates of CH_4 emission, oxidation efficiencies, and dilution rates along other parts of the USAM, particularly between the region of widespread emission between Wilmington Canyon and Cape Hatteras.

5. Conclusions

Measurements of dissolved CH_4 concentration, oxidation rates, and current velocity were considered with a steady state box model to estimate the release rate of CH_4 at the updip limit of clathrate hydrate stability in Hudson Canyon. A sensitivity analysis was conducted to encompass likely spatial and temporal variations in CH_4 emission, as well as artifacts in the measurement parameters incorporated into the model. This analysis suggests that on average 69 (35–138) Mg CH_4 y^{-1} (possibly as large as 70–280 Mg CH_4 y^{-1} for the entire Hudson Canyon) is being emitted updip of hydrate stability in Hudson Canyon. While further investigation is necessary to determine the total amount of CH_4 being released along the U.S. Atlantic Margin and its influence on ocean chemistry and greenhouse gas fluxes, the analyses presented here suggest moderate emission rates, similar to mean values for marine CH_4 seeps, currently exist in this region.

Acknowledgments
This research was funded by the National Science Foundation OCE-1318102 to J.D. Kessler. This work was supported in part by a fellowship in ocean sciences from the Sloan foundation to J.D. Kessler. T.C. Weber was supported by U.S. Department of Energy award DE-FE0013999 and NSF OCE-1352301. C. Ruppel was partially supported by DOE-USGS interagency agreements DE-FE0002911 and DE-FE0005806. The data presented in this work can be found in the supporting information, while all underway and CTD data sets from this expedition are freely available on the Rolling Deck to Repository (R2R) website found at http://www.rvdata.us/catalog/EN541 (doi:10.7284/903242). We thank Katy Sparrow, Mengran Du, Alexandre Chepigin, Bethany Rosemore, and Arielle Green for help with at-sea sample collection, Nick Huynh for laboratory assistance, as well as the captain, crew, and Bill Fanning of the R/V *Endeavor* for unending enthusiasm, professionalism, and support at sea. Any use of trade names is for descriptive purposes and does not imply endorsement by the U.S. government. A. Weinstein and L. Navarrete contributed equally to this work.

References

Archer, D. (2007), Methane hydrate stability and anthropogenic climate change, *Biogeosciences*, *4*(4), 521–544.

Brothers, L. L., C. L. Van Dover, C. R. German, C. L. Kaiser, D. R. Yoerger, C. D. Ruppel, E. Lobecker, A. D. Skarke, and J. K. S. Wagner (2013), Evidence for extensive methane venting on the southeastern U.S. Atlantic margin, *Geology*, *41*(7), 807–810, doi:10.1130/G34217.1.

Burdic W. S. (1991), *Underwater Acoustics System Analysis*, pp. 366–368, Prentic Hall, Englewood Clliffs, N. J.

Butman, B., D. C. Twichell, P. A. Rona, B. E. Tucholke, T. J. Middleton, and J. R. Robb (2006), Sea floor topography and backscatter intensity of the Hudson Canyon region offshore of New York [CD-ROM], *U.S. Geol. Surv. Open File Rep.*, *2004-1441*, Version 2.0. 1. [Available at http://pubs.usgs.gov/of/2004/1441/index.html.]

Dickens, G. R., and M. S. Quinby-Hunt (1994), Methane hydrate stability in seawater, *Geophys. Res. Lett.*, *21*(19), 2115–2118, doi:10.1029/94GL01858.

Dickens, G. R., J. R. Oneil, D. K. Rea, and R. M. Owen (1995), Dissociation of oceanic methane hydrate as a cause of the carbon-isotope excursion at the end of the Paleocene, *Paleoceanography*, *10*(6), 965–971, doi:10.1029/95PA02087.

Graves, C. A., L. Steinle, G. Rehder, H. Niemann, D. P. Connelly, D. Lowry, R. E. Fisher, A. W. Stott, H. Sahling, and R. H. James (2015), Fluxes and fate of dissolved methane released at the seafloor at the landward limit of the gas hydrate stability zone offshore western Svalbard, *J. Geophys. Res. Oceans*, *120*, 6185–6201, doi:10.1002/2015JC011084.

Greinert, J., Y. Artemov, V. Egorov, M. De Batist, and D. McGinnis (2006), 1300-m-high rising bubbles from mud volcanos at 2080 m in the Black Sea: Hydroacoustic characteristics and temporal variability, *Earth Planet. Sci. Lett.*, *244*(1/2), 1–15, doi:10.1016/j.epsl.2006.02.01.

Hornafius, J., D. Quigley, and B. Luyendyk (1999), The world's most spectacular marine hydrocarbon seeps (Coal Oil Point, Santa Barbara Channel, California): Quantification of emission, *J. Geophys. Res.*, *104*(C9), 20,703–20,711, doi:10.1029/1999JC900148.

Hovland, M., A. G. Judd, and R. A. Burke (1993), The global flux of methane from shallow submarine sediments, *Chemosphere*, *26*(1–4), 559–578.

Jerram, K., T. C. Weber, and J. Beaudoin (2015), Split-beam echo sounder observations of natural methane seep variability in the northern Gulf of Mexico, *Geochem. Geophys. Geosyst.*, *16*, 736–750, doi:10.1002/2014GC005429.

Kennett, J. P., K. G. Cannariato, I. L. Hendy, and R. J. Behl (2000), Carbon isotopic evidence for methane hydrate instability during quaternary interstadials, *Science*, *288*(5463), 128–133, doi:10.1126/science.288.5463.128.

Kessler, J. D. (2014), Seafloor methane: Atlantic bubble bath, *Nat. Geosci.*, *7*(9), 625–626, doi:10.1038/ngeo2238.
Kessler, J. D., W. S. Reeburgh, J. Southon, and R. Varela (2005), Fossil methane source dominates Cariaco Basin water column methane geochemistry, *Geophys. Res. Lett.*, *32*, L12609, doi:10.1029/2005GL022984.
Kessler, J. D., W. S. Reeburgh, J. Southon, R. Seifert, W. Michaelis, and S. C. Tyler (2006a), Basin-wide estimates of the input of methane from seeps and clathrates to the Black Sea, *Earth Planet Sci. Lett.*, *243*(3/4), 366–375, doi:10.1016/j.epsl.2006.01.006.
Kessler, J. D., W. S. Reeburgh, and S. C. Tyler (2006b), Controls on methane concentration and stable isotope (δ^2H-CH_4 and δ^{13}C-CH_4) distributions in the water columns of the Black Sea and Cariaco Basin, *Global Biogeochem. Cycles*, *20*, GB4004, doi:10.1029/2005GB002571.
Leonte, M., J. D. Kessler, A. Chepigin, T. Weber, C. Ruppel, M. Y. Kellermann, E. Arrington, D. L. Valentine, and S. P. Silva (2014), Comparison of two techniques to calculate methane oxidation rates in samples obtained from the Hudson Canyon seep field in the north Atlantic, Abstract B51J-0135 presented at 2014 AGU Fall Meeting, AGU, San Francisco, Calif., 15–19 Dec.
Lentz, S. J. (2008a), Observations and a model of the mean circulation over the Middle Atlantic Bight continental shelf, *J. Phys. Oceanogr.*, *38*(6), 1203–1221, doi:10.1175/2007JPO3768.1.
Lentz, S. J. (2008b), Seasonal variations in the circulation over the Middle Atlantic Bight continental shelf, *J. Phys. Oceanogr.*, *38*(7), 1486–1500, doi:10.1175/2007JPO3767.1.
Mau, S., J. Blees, E. Helmke, H. Niemann, and E. Damm (2013), Vertical distribution of methane oxidation and methanotrophic response to elevated methane concentrations in stratified waters of the Arctic fjord Storfjorden (Svalbard, Norway), *Biogeosciences*, *10*(10), 6267–6278, doi:10.5194/bg-10-6267-2013.
Merewether, R., M. S. Olsson, and P. Lonsdale (1985), Acoustically detected hydrocarbon plumes rising from 2-km depths in the Guayamas Basin, Gulf of California, *J. Geophys. Res.*, *90*(NB4), 3075–3085, doi:10.1029/JB090iB04p03075.
Milkov, A. V. (2004), Global estimates of hydrate-bound gas in marine sediments: How much is really out there?, *Earth Sci. Rev.*, *66*(3–4), 183–197, doi:10.1016/j.earscirev.2003.11.002.
Milkov, A. V., G. R. Dickens, G. E. Claypool, Y.-J. Lee, W. S. Borowski, M. E. Torres, W. Xu, H. Tomaru, A. M. Tréhu, and P. Schultheiss (2004), Co-existence of gas hydrate, free gas, and brine within the regional gas hydrate stability zone at Hydrate Ridge (Oregon margin): Evidence from prolonged degassing of a pressurized core, *Earth Planet Sci. Lett.*, *222*(3/4), 829–843, doi:10.1016/j.epsl.2004.03.028.
NOAA National Centers for Environmental Information (2004), Multibeam Bathymetry Database (MBBDB), cruises EX1205, EX1206, EX1302, EX1303, EX1403, EX1404. NOAA National Centers for Environmental Information. doi:10.7289/V56T0JNC.
Pack, M. A., M. B. Heintz, W. S. Reeburgh, S. E. Trumbore, D. L. Valentine, X. M. Xu, and E. R. M. Druffel (2011), A method for measuring methane oxidation rates using low-levels of ^{14}C-labeled methane and accelerator mass spectrometry, *Limnol. Oceanogr. Methods*, *9*, 245–260, doi:10.4319/lom.2011.9.245.
Pierdomenico, M., V. G. Guida, L. Macelloni, F. L. Chiocci, P. A. Rona, M. I. Scranton, V. Asper, and A. Diercks (2015), Sedimentary facies, geomorphic features and habitat distribution at the Hudson Canyon head from AUV multibeam data, *Deep Sea Res., Part II*, *121*, 112–125, doi:10.1016/j.dsr2.2015.04.016.
Rona, P., V. Guida, M. Scranton, D. L. Gong, L. Macelloni, M. Pierdomenico, A. R. Diercks, V. Asper, and S. Haag (2015), Hudson submarine canyon head offshore New York and New Jersey: A physical and geochemical investigation, *Deep Sea Res., Part II*, *121*, 213–232, doi:10.1016/j.dsr2.2015.07.019.
Ruppel, C. (2011), Methane hydrates and contemporary climate change, *Nat. Educ. Knowl.*, *3*(10), 29.
Scranton, M. I. (1988), Temporal variations in the methane content of the Cariaco Trench, *Deep Sea Res., Part A*, *35*(9), 1511–1523, doi:10.1016/0198-0149(88)90100-8.
Scranton, M. I., F. L. Sayles, M. P. Bacon, and P. G. Brewer (1987), Temporal changes in the hydrography and chemistry of the Cariaco Trench, *Deep Sea Res., Part A*, *34*(5/6), 945–963, doi:10.1016/0198-0149(87)90047-1.
Skarke, A., C. Ruppel, M. Kodis, D. Brothers, and E. Lobecker (2014), Widespread methane leakage from the sea floor on the northern US Atlantic margin, *Nat. Geosci.*, *7*(9), 657–661, doi:10.1038/ngeo2232.
Tréhu, A. M., P. B. Flemings, N. L. Bangs, J. Chevallier, E. Gràcia, J. E. Johnson, C.-S. Liu, X. Liu, M. Riedel, and M. E. Torres (2004), Feeding methane vents and gas hydrate deposits at south Hydrate Ridge, *Geophys. Res. Lett.*, *31*, L23310, doi:10.1029/2004GL021286.
Valentine, D. L., et al. (2010), Propane respiration jump-starts microbial response to a deep oil spill, *Science*, *330*(6001), 208–211, doi:10.1126/science.1196830.
Valentine, D. L., I. Mezić, S. Maćešić, N. Črnjarić-Žic, S. Ivić, P. J. Hogan, V. A. Fonoberov, and S. Loire (2012), Dynamic autoinoculation and the microbial ecology of a deep water hydrocarbon irruption, *Proc. Natl. Acad. Sci. U. S. A.*, *109*(50), 20,286–20,291, doi:10.1073/pnas.1108820109.
Warner, J. C., B. Armstrong, R. Y. He, and J. B. Zambon (2010), Development of a coupled ocean-atmosphere-wave-sediment transport (COAWST) modeling system, *Ocean Modell.*, *35*(3), 230–244, doi:10.1016/j.ocemod.2010.07.010.
Weber, T. C., L. Mayer, K. Jerram, J. Beaudoin, Y. Rzhanov, and D. Lovalvo (2014), Acoustic estimates of methane gas flux from the seabed in a 6000 km^2 region in the Northern Gulf of Mexico, *Geochem. Geophys. Geosyst.*, *15*, 1911–1925, doi:10.1002/2014GC005271.
Westbrook, G. K., et al. (2009), Escape of methane gas from the seabed along the West Spitsbergen continental margin, *Geophys. Res. Lett.*, *36*, L15608, doi:10.1029/2009GL039191.
Wiesenburg, D. A., and N. L. Guinasso (1979), Equilibrium solubilities of methane, carbon monoxide, and hydrogen in water and sea water, *J. Chem. Eng. Data*, *24*(4), 356–360, doi:10.1021/je60083a006.
Yvon-Lewis, S. A., L. Hu, and J. Kessler (2011), Methane flux to the atmosphere from the Deepwater Horizon oil disaster, *Geophys. Res. Lett.*, *38*, L01602, doi:10.1029/2010GL045928.